Low Complexity Fast Direct Solution for Multiscale Problems with Nested Equivalence Source Approximation

A Microwave Sensing System Based on Transmitarray Antennas for Detecting Low-Density Contaminants in Food Packaged Products

Yuhan Zuo, Qijian Lu, Weiliang Yu, Rui Chen, *Member, IEEE*, Pengfei Gu, Mengmeng Li, *Senior Member, IEEE*, Francesca Vipiana, *Senior Member, IEEE*, Dazhi Ding, *Senior Member, IEEE*

***Abstract*—A novel microwave sensing (MWS) system for detecting low-density contaminants in food packaged products is presented in this work. The proposed MWS system is featured by a pair of transmitarray antennas designed at 10 GHz with electrically reconfigurable unit cells. The focus spot of the transmitarray antennas can be scanned and focused at the desired positions along the horizontal or vertical direction in their near-field region. Compared with existing standard MWS systems with fixed waves, the proposed MWS system has a larger and more flexible near-field detection coverage. Moreover, the electric field is enhanced by the transmitarray, which contributes to a better detection. Then, we design a machine learning model, based on the proposed transmitarray antenna, to detect the different low-density contaminants in static oil-filled food jars. Experimental results demonstrate improved performance in the detection accuracy where 100% and 99% are observed with different scanning strategies with the proposed system, while less than 90% with the existing standard ones.**

***Index Terms*—Antenna arrays, food inspection, low-density contaminans, microwave sensors, machine learning.**

I. Introduction

In the last few decades, food quality and safety has gained more and more attention due to the increasing diverse and complex types of the food [1]–[3]. Food contaminant inspection is a necessary step for ensuring the food safety. Among different techniques for the food contaminant inspection, X-ray and metal detectors are the two most widely used methods [4]. However, X-ray techniques have limited detection capabilities for the detection of low-density contaminants, such as plastic ones, and may be harmful to operators. On the other hand, metal detectors are only applicable for detecting metal objects while most contaminants in the food packages are non-metallic materials, such as plastic, wood and glass.

In recent years, microwave sensing (MWS) techniques have been developed for the detection of the food contaminants by addressing the issues of the above traditional food inspection methods [5]–[9]. The MWS techniques identify or even image the contaminants in the food by analyzing the electromagnetic responses (e.g., electric field and S-parameters) of the food with and without the contaminants. The imaging of the food contaminants usually requires both the electric field and S-parameters at the antenna ports to obtain the solution of the electromagnetic inverse problems [8], [10]–[11]. In [8], a noninvasive MWS system has been developed for imaging metal and plastic contaminants inside hazelnut–cocoa cream-based food jars, which is composed of a pair of horn antennas for the measurement of the S-parameters at the antenna ports. The frequency is ranging from 9 to 11 GHz considering the tradeoff between the electromagnetic penetration depth for the oil and the detection resolution for the contaminants. However, since the measurements are only taken along the conveyor belt direction, there are some replicas in the obtained images of the food contaminants. To obtain more information from the measured S-parameters, another multi-view MWS system with six antennas is designed in [10]. To further expand the scope for inspections with different food materials, a wideband imaging system is proposed in [27] for both water-based and oil-based products. In addition, other MWS systems are presented in [12] for the food imaging along the production line with short detection time and limited measurement data. However, the identification from the imaging of the food contaminants using the MWS system usually requires the complex solution of the electromagnetic inverse problems, and due to the inability to measure electric fields in food, it can be difficult to be achieved in realistic applications.

Therefore, identifying the existence of the food contaminants without imaging using the MWS system is more

This work was supported in part by National Natural Science Foundation of China (NSFC) under Grant 32261133623, 62201264, 61890541, 62222108, and 62331016; in part by "INSIGHT-FOOD, An innovative microwave sensing system for the evaluation and monitoring of food quality and safety" (CUP E13C230001800005), a joint research project within the Executive Program of Scientific and Technological Cooperation between Italy and China (period 2023-2025), funded by NSFC and MAECI; in part by the Fundamental Research Funds for the Central Universities under Grant 30921011101 and 30924010207; in part by the Fund Program for the Scientific Activities of Selected Returned Overseas Professionals in Shanxi Province under Grant 20240063. *(Corresponding author: Dazhi Ding.)*

Y. Zuo, Q. Lu, W. Yu, P. Gu, M. Li, and D. Ding are with the School of Microelectronics (School of Integrated Circuits), Nanjing University of Science and Technology, Nanjing 210094, China (e-mail: limengmeng@njust.edu.cn; dzding@njust.edu.cn).

R. Chen is with the School of Microelectronics (School of Integrated Circuits), Nanjing University of Science and Technology, Nanjing 210094, China and also with the North Automatic Control Technology Institute, Taiyuan 030006, China (e-mail: rui.chen@njust.edu.cn).

F. Vipiana is with the Department of Electronics and Telecommunications, Politecnico di Torino, 10129 Torino, Italy (francesca. vipiana@polito.it).

convenient and straightforward by analyzing the only S-parameters of the food with and without the contaminants. The review of [12] points out that machine learning is a powerful method to relate microwave signals to food quality and safety, and the identifications are made by indicating the food in the image with most of the existing systems. Some MWS systems based on the machine learning (ML) techniques have been developed for the real-time detection of the food contaminants [13]–[18]. For example, the multilayer perceptron (MLP) and non-linear support vector machine (SVM) algorithms have been used with the S-parameters as the input data for the training and testing of the ML models. However, these MWS systems are composed of the antennas that have the fixed waves resulting in limited coverage for the food inspection, which provide less spatial information with in the detection range. This also poses a challenge to the hardware of the system in a realistic production line as the data should be obtained before the food is moved out of the detection domain. In addition, as the wave is not focused to the food being tested, it is not guaranteed that the actual wave entering the interior of the food is enough for the detection.

Here, we propose an MWS system based transmitarray antennas that, to the best of our knowledge, have never been used, in open literature, for detecting contaminants in food packaged items along the production line. The use of transmitarray antennas will address the issues of the limited detection domain and wave penetration capability, compared with the existing standard MWS systems. We also apply the machine learning in the identifications but in another way, as the input is the scattering parameters, not the images. The novelty could be indicated by the usage of the flexibility of the transmitarray which is very suitable for food inspection. The integration of the entire system including the transmitarray regulated by the FPGA, the VNA for generating raw S-parameters data, the algorithm to construct each sample by the S-parameters data and the machine learning model for classification is the new contribution of our work and potentially provides a novel solution to the food inspection in industry.

The proposed MWS system is composed of one radiating horn antenna, one receiving horn antenna, two 10 GHz transmitarray antennas based on electrically reconfigurable metasurface arrays, and one 2-port vector network analyzer (VNA) for the S-parameter measurement. By manipulating the on/off state of the PIN diodes loaded on the unit cells of the metasurface arrays [19]–[22], the electromagnetic waves transmitted by the transmitarray antennas can be scanned and focused at different desired positions along the horizontal and vertical directions in the near-field region. Compared with the existing standard antenna array systems with only the fixed-waves antennas, the proposed MWS system has a more flexible focus spot control which allows customized EM wave focusing and scanning designs for different kinds of food without changing the antenna configuration. Furthermore, the larger coverage for the food inspection can provide more spatial information for detecting potential contaminants.

In addition, we develop a ML model with neural network (NN) to classify the different types and the different locations of the low-density contaminants in the food jars. Taking a static oil-filled food jar with three kinds of contaminants as an example, experimental results are presented to demonstrate the more advanced performance for the detection of the contaminants. With our presented MWS system, the classification accuracy for different contaminant kinds can reach almost 100%, while less than 90% accuracy using only a pair of horn antennas without the transmitarray. Some similar systems have been proposed based on transmitarrays for other types of applications [24], [25]. The application in [25] is mainly about imaging of breast tissues without any diagnosis for unhealthy results compared with the healthy ones. Compared with these systems, we develop a machine learning model beyond imaging for identifying the existence of contaminants in food jars from the uncontaminated ones, as identifying whether the food item is contaminated or not should be more important than imaging the contaminants. The identification is more according with the industrial needs than just imaging. Another significant difference is that many applications with transmit-arrays are designed for static targets (e.g., breast tissues in [25]) while our proposed system is for fast moving food jars in a production line. Therefore, there are strict requirements for the speed of the beamforming and the switching capability with the transmit-array and the FPGA in our system which will be elaborated in the following text. Furthermore, some other microwave systems are proposed for applications such as the stroke monitoring in the medical industry [26]. The work of [26] requires initial image data to estimate the spatial dimensions of the stroke region together with the scattering parameter data. In our work, only scattering parameter data are required for generating the dataset as our purpose is to classify, not to reconstruct the spatial information of the contaminants. In terms of the same application for detecting contaminants, the proposed system can be seen as a further improved version of a multi-antenna system with a more flexible wave control capability and a customized spot focusing strategy which significantly improves the electric field inside the food. Furthermore, different from [8] and [10] which are for imaging, a machine learning model is designed with our proposed system for classification.

The remainder of this paper is organized as follows. In Sect. II, we introduce the background and the design of the MWS system. In addition, we present the design and the phase manipulation of the unit cell of the transmitarry antenna as well as the fabrication of the transmitarray antenna. Then, the simulation results for the comparison of the performance of the designed transmitarray antenna and the horn antenna are present. Subsequently, the near-field performance of the transmitarray antenna is investigated by the measurements in Sect. III. To describe the developed NN, we also present the generation of the datasets, the construction of the NN, the training and testing of the NN. Finally in Sect. IV, we conclude this work along with the perspectives.

In [23], a preliminary version of the transmitarray antenna has been presented.

II. The MWS System

A. Background

First of all, we would like to introduce the background of the MWS technique for identifying the existence of the contaminants in the food jars. Assuming a food jar without the contaminant and that with the contaminant are illuminated by the same electromagnetic wave generated from the radiating antenna feed source, S-parameters are obtained from the electromagnetic waves received by the receiving antenna for the two food jars. The difference of the S-parameters for the two cases, ΔS , can be approximately expressed using the dielectric contrast, $\Delta\chi(\boldsymbol{r})$, as [8]:

$$\Delta S(\boldsymbol{r}_p,\boldsymbol{r}_q) \approx \frac{-j\omega\varepsilon_b}{2a_p a_q}\int_R \boldsymbol{E}_b(\boldsymbol{r}_p,\boldsymbol{r})\cdot\boldsymbol{E}_b(\boldsymbol{r},\boldsymbol{r}_q)\Delta\chi(\boldsymbol{r})d\boldsymbol{r} \quad (1)$$

where $\boldsymbol{r}_p$ and $\boldsymbol{r}_q$ are the positions of the receiving and transmitting antennas, a_p and a_p are the known incoming waves at the antenna ports respectively. ε_b is the complex permittivity of the medium filled in the food jars, ω is the angular frequency, R is the region of interest, $\Delta\chi = \Delta\varepsilon / \varepsilon_b$ is the dielectric contrast defined as the ratio of the difference between ε_b and the permittivity of the contaminant, $\boldsymbol{E}_b(\boldsymbol{r}_p,\boldsymbol{r})$ and $\boldsymbol{E}_b(\boldsymbol{r},\boldsymbol{r}_q)$ are the radiated electric field at $\boldsymbol{r}$ by the antennas located in $\boldsymbol{r}_p$ and $\boldsymbol{r}_q$, respectively, for the food jar without the contaminants. Note that, the distorted Born approximation [8] is applied in (1) since the size of the contaminant is generally much smaller than that of the food jar, i.e. the domain of interest. It can be found in (1), as long as $\Delta\chi(\boldsymbol{r})$ is non-zero, there exists a non-zero value ΔS . Therefore, the existence of the contaminant can be identified from the difference of the S-parameters of the food jars with and without the contaminants.

B. Design of the MWS System

The near-field and far-field are divided according to the distance $\frac{2D^2}{\lambda}$, where D is the aperture size of the antenna array and λ is the wavelength. In our system, D is 0.3m and λ is 0.03m (corresponding to 10 GHz), therefore:

$$\frac{2D^2}{\lambda} = \frac{2\times 0.3^2}{0.03} = 6m$$

In the experiments, we set the width of the production line to be 1m which is also the distance of the two arrays, so the distance from the array to the center point of the production line is 0.5m and should be regarded as near-field. Therefore, the MWS system should be defined for the near-field.

The MWS system proposed in this work consists of a radiating horn antenna, a receiving horn antenna, two 10 GHz transmitarray antennas based on electrically reconfigurable metasurface arrays, and a 2-port VNA for the S-parameter measurement as shown in Fig. 1. In our MWS system, the vertical polarization is used. The linear polarization has been also used in previous works in [8] and [14] for detecting contaminants, and we have not observed significant differences between the vertical and horizontal polarizations. It is worth noting that our proposed system is a general method and one can also design systems with different unit cell structures with other polarizations.

The operation frequency band of the proposed MWS system is set between 9.5 and 10.5 GHz centered at 10 GHz. In the case of water-based products, the same system could be used but at the lower frequencies due to the higher losses within the product. It is worth noting that, for detecting the contaminants in the static oil-filled food jars, we assume only one food jar is placed within the detection region for each S-parameter measurement to avoid the interference from the other food jars.

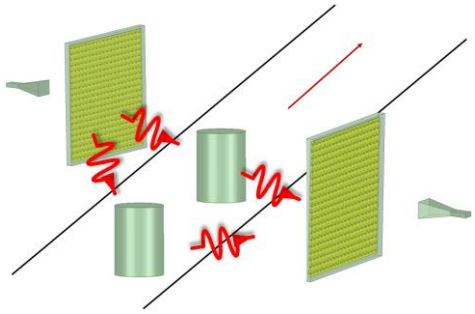

Fig. 1. The schematic diagram of the proposed MWS system in a production line.

C. Design of the Unit Cell of the Transmitarray Antenna

The designed 10 GHz transmitarray antenna is composed of 20×20 electrically reconfigurable unit cells loaded with the PIN diodes. The 1-bit unit cell is composed of two F4BTMS350 dielectric substrate layers, two (transmitting and receiving) copper microstrip layers, two middle copper ground layers, and one Rogers RO4450F adhesive plate layer. The receiving metal microstrip layer is composed of a side feeding loop antenna while the transmitting metal microstrip layer is composed of a loop antenna and two PIN diodes. The structure and the dimension of the designed 1-bit unit cell are shown in Fig. 2.

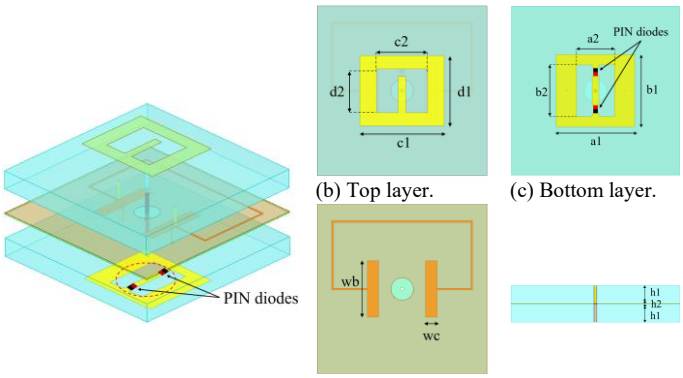

(a) Overall structure. (b) Top layer. (c) Bottom layer. (d) Interlayer. (e) Front view.

Fig. 2. Schematic diagram of transmitarray antenna unit; a1=6.9, a2=3.4, b1=6.4, b2=4.6, c1=7.4, c2=4.5, d1=6.2, d2=3.9, wb=5, wc=1, h1=1.6, h2=0.2; all the lengths are in millimeter. PIN diodes are marked in the figure.

The materials used for the design of the unit cell introduce the loss of the electromagnetic wave that affects the transmission efficiency of the unit cell. To investigate the attenuation effect of the electromagnetic wave transmitted through the unit cell, we use the HFSS software with the master slave boundary conditions to simulate the S-parameters of the unit cell with the incident electromagnetic wave at different states (on and off) of the PIN diodes over the whole frequency band as shown in Fig. 3. As shown in Fig. 3(a) and (b), within the whole frequency band, the amplitudes of the S_{12} parameters (i.e., transmission coefficients) are over -2.5 dB and the difference of the phases of the S_{12} parameters for the on and off states of the PIN diodes maintains almost 180°, which satisfies the design requirement for the attenuation of the electromagnetic wave. Note that, the phases of the S_{12} parameters for the on and off states of the PIN diodes are different since the PIN diodes can control the flow direction of the current on the unit cell.

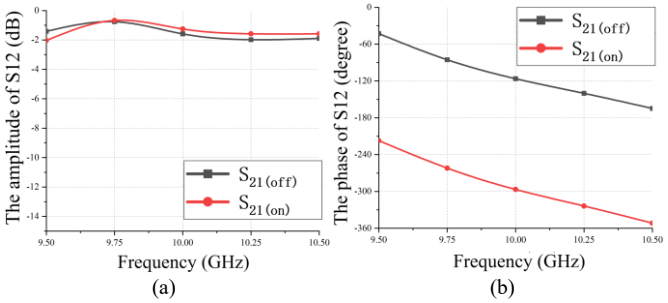

(a) (b)

Fig. 3. The amplitude (a) and phase (b) of the S_{12} parameters of the unit cell with the incident electromagnetic wave at different states of the PIN diodes over the frequency band.

D. Phase Manipulation of the Unit Cell

The spot focusing and scanning of the transmitarray antenna at different positions in near-field can be achieved by controlling the on/off states of the PIN diodes of all the 400 unit cells. By adjusting the transmission phase of the unit cell, we can compensate the phase delay due to the spatial distance between the feed source and the unit cell. For the 1-bit unit cell located at the m-th row and the n-th column of the transmitarray antenna, the actual phase compensation $\varphi_c(m,n)$ of the PIN diodes can be quantified by $\phi_c(m,n)$ compared with the reference phase $\varphi(1,1)$ given by

$$\phi_c(m,n)=\begin{cases} 0^\circ, -90^\circ+2k\pi<\varphi_c(m,n)\leqslant 90^\circ+2k\pi \\ 180^\circ, 90^\circ+2k\pi<\varphi_c(m,n)\leqslant 270^\circ+2k\pi \end{cases} k=0,\pm1,\pm2,\cdots \quad (2)$$

where m and n are the location indices of the row and column for the unit cell respectively. Note that, since we use the 1-bit unit cell, the unit cell has only two discrete states (on and off). Here we only design the phases of the unit cells to achieve a focusing effect at the desired positions and no other algorithm is used for the beamforming

To illustrate the phase manipulation of the unit cells of the transmitarray antenna, Fig. 4(a)-(d) presents the actual and quantified phase compensation distributions of the unit cells for the E-plane spot focusing and scanning at the different locations at 10GHz. The permittivity of the food jar has not been taken into account and the system is designed to focus the electric field within the detection domain in free space where the jars are expected to be. Here, we use "0" for denoting 0° quantified phase compensation and "1" for denoting 180° quantified phase compensation as shown in Fig. 4(b) and (d) with different focusing positions.

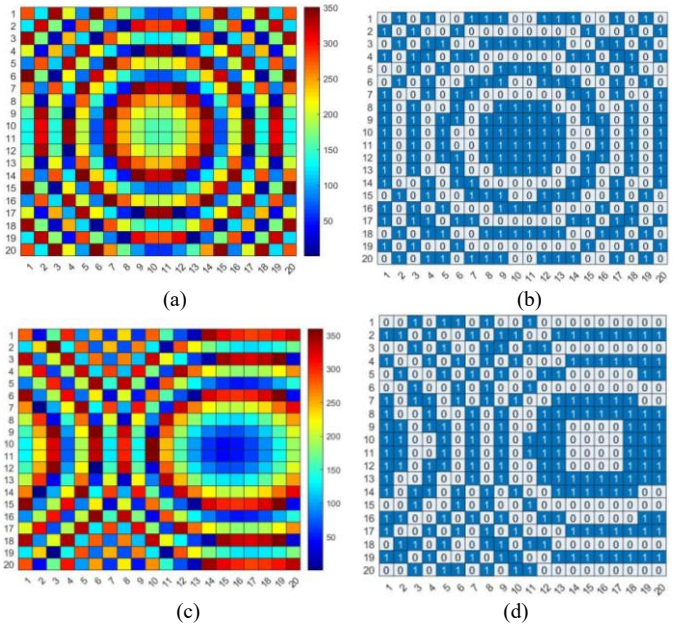

(a) (b) (c) (d)

Fig. 4. Theoretical ((a), (c)) and actual ((b), (d)) compensation phase distribution at 10 GHz for the center position ((a), (b)) and for the right position ((c), (d)) within the detection range.

E. Transmitarray Antenna Simulation Results

In this section, we present the simulation results using the HFSS software to investigate the near-field performance of the transmitarray antenna.

First, with the focusing strategy along both horizontal and vertical directions, we take three horizontal positions (left, middle and right) at three vertical positions (upper, center and lower) for simulations. We simulate the electric field within the three rectangular simulation planes in size of 10×20 cm where the food jar is expected to be located (larger than the size of the cross section of the cylindrical food jar 8×18 cm) 50 cm away from the transmitarray antenna. We set the left as the positive direction and the right as the negative direction, and the center points of the three simulation planes along the horizontal direction are 10 cm, 0 cm, and -10 cm shift from the center of the transmitarray antenna along the horizonal direction. For each plane, we simulate the electric field for the spots focused at the upper, center, and lower locations with the interval of 6 cm along the vertical direction. To begin with, we present the computed electric field distribution generated by superposing the array factor contributions from equivalent ideal point sources using the theoretical phases in Fig. 5 (a)-(i) and using the quantified phases in Fig. 5 (j)-(r) as a comparison. Then, we construct the actual array model with circuits where the source is a realistic horn and simulate the

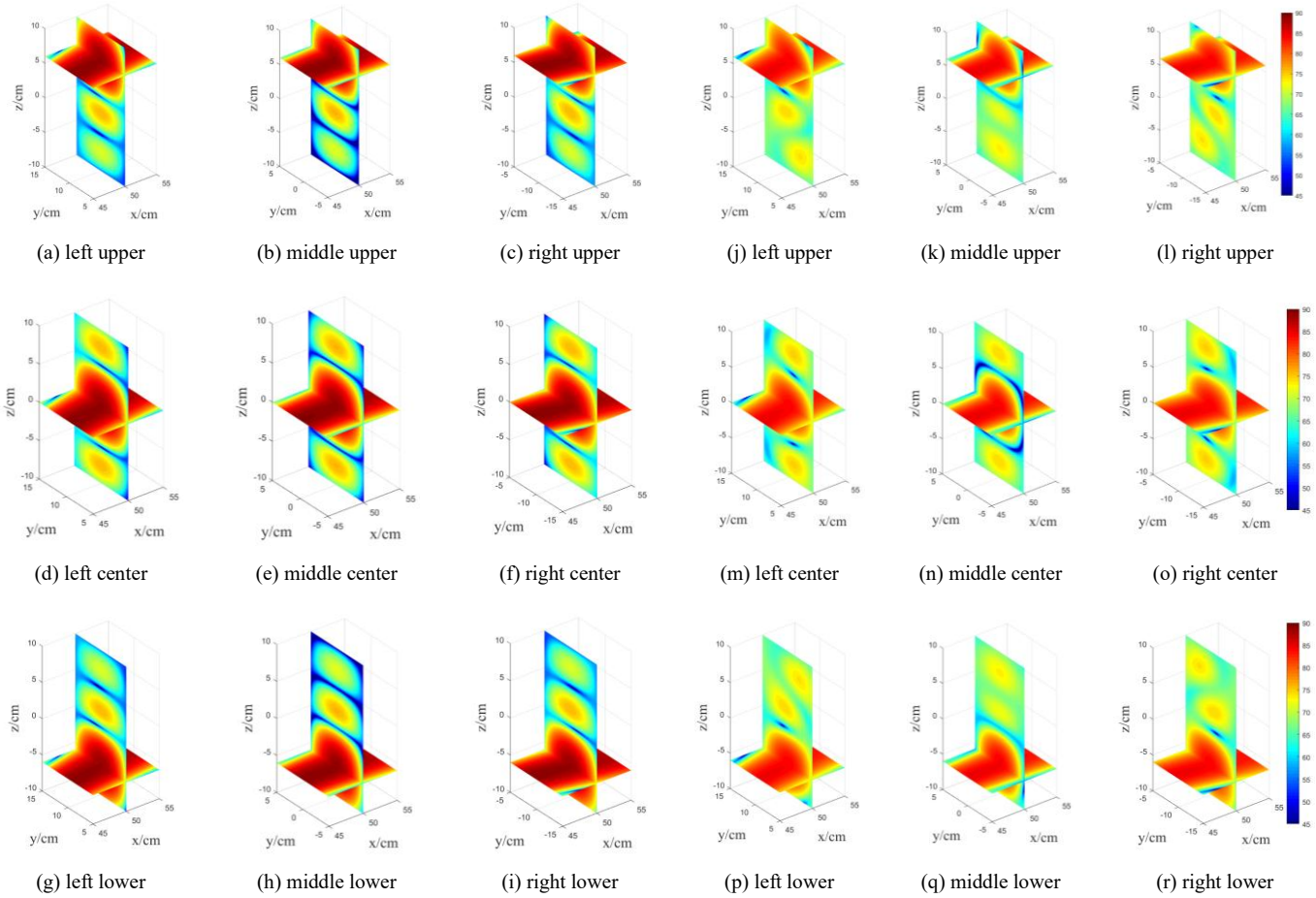

(a) left upper (b) middle upper (c) right upper (j) left upper (k) middle upper (l) right upper

(d) left center (e) middle center (f) right center (m) left center (n) middle center (o) right center

(g) left lower (h) middle lower (i) right lower (p) left lower (q) middle lower (r) right lower

Fig. 5. The electric field intensity at the left ((a)(d)(g)), the middle ((b)(e)(h)) and the right ((c)(f)(i)) positions focusing at the upper, center and lower positions obtained by theoretical phases and the electric field intensity at the left ((j)(m)(p)), the middle ((k)(n)(q)) and the right ((l)(o)(r)) positions focusing at the upper, center and lower positions obtained by quantified phases from the computation. The electric field is calculated by superposing the array factor contributions from equivalent ideal point sources. The electric fields are expressed in units of V/m.

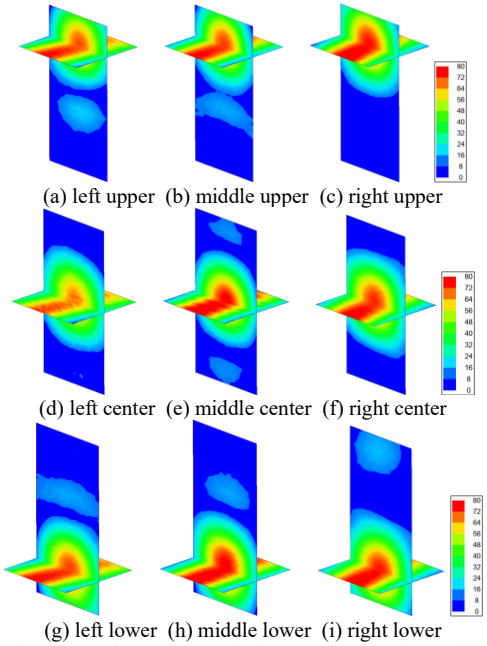

(a) left upper (b) middle upper (c) right upper

(d) left center (e) middle center (f) right center

(g) left lower (h) middle lower (i) right lower

Fig. 6. The electric field intensity at the left ((a)(d)(g)), the middle ((b)(e)(h)) and the right ((c)(f)(i)) positions focusing at the upper, center and lower positions obtained by quantified phases from the simulation for the array model with circuits where the source is a realistic horn. The electric fields are expressed in units of V/m.

field with quantified phases as shown in Fig. 6.

From the electric field results in Fig. 5 and Fig. 6, we conclude that the actual focusing positions obtained by simulation with quantified phases are consistent with the positions obtained by computation with theoretical phases. The spot dimensions obtained by both distributions are similar, which both cover the detection domain where the jars are expected to be. Nevertheless, the E-field values of Fig. 5 (j)-(r) and Fig. 6 are not exactly consistent mainly because the results are from different models where the sources are different. Mutual couplings between closely spaced units and the mesh discretization errors for the horn and the array model can also cause realistic simulation differences compared with the theoretical analysis. In addition, we observe that there are periodic focusing spots in the computed field produced by the theoretical phases. Actually, the periodic focusing observed with theoretical continuous phase modulation arises from strong near-field spatial coherence, whereas the 1-bit quantified phase suppress the coherent interference from the focus, resulting in a more localized focusing distribution. From the horizontal planes we find that the focusing electric field is continuous and extended along the horizontal direction. As a comparison, Fig. 7 presents the simulated electric field

within the simulation plane for the spot focused at the center position using only the horn antenna (without the transmitarray antenna).

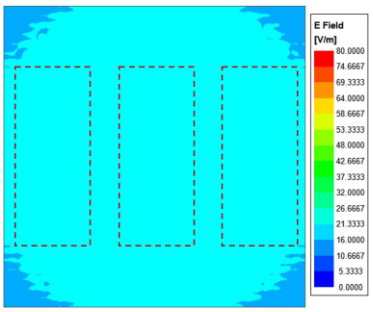

Fig. 7. The electric field intensity induced by the horn. The cross section of the jar at left, middle and the right positions are marked by the red dashed boxes.

Furthermore, we simulate the electric field within the of the cross section inside an actual cylindrical oil jar located 50 cm away from the transmitarray antenna, to verify that the focusing can enhance the electric field intensity in a food jar. Figure 8 compares the simulated electric field of the cross section inside the oil-filled cylindrical food jar with and without the transmitarray antenna for the spot focused at the center position. It clearly shows that the electric field inside the food jar with the transmitarray antenna is higher than that with only the horn antenna. It needs to be mentioned that, as inferred from (1), for the same difference of the dielectric constants, the higher electric field inside the domain of interest results in the larger difference of the S-parameters, which can be helpful for the food contaminant detection.

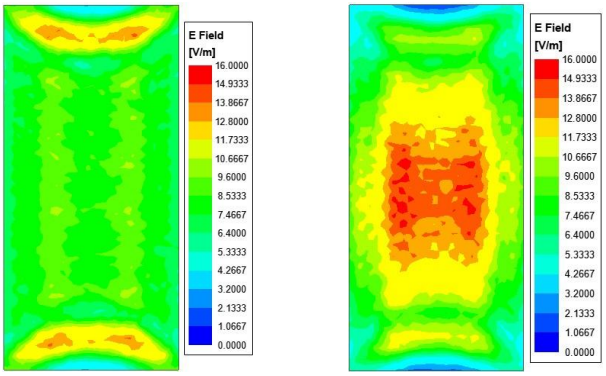

(a) (b)

Fig. 8. Electric field inside an actual presented food jar filled with oil; (a) without and (b) with the transmitarray antenna. The size of the cross section is 8cm×18cm.

F. Fabrication of the Transmitarray Antenna

After the design of the transmitarray antenna, we describe the fabrication of the antenna using the printed circuit board (PCB). The PCB is made up of four metal layers, i.e., the active patch layer (top), the passive patch layer (bottom), the DC bias line wiring layer for controlling diodes (middle-1), and the layer for isolating the electromagnetic waves and the common ground terminal design for the diodes (middle-2). The layout of the layers of the PCB are shown in Fig. 9.

To automatically control the on/off states of the PIN diodes of the 400 unit cells, we design a FPGA system for the independent control (i.e., the point control) for the transimitarray antenna. The schematic diagram of the control board of the FPGA system is shown in Fig. 10(a). The DC power bias voltage supplied for the FPGA system is 12 V. The encoding matrix of the controlled focus spot states obtained from the upper computer is sent to the memory of the lower computer of the FPGA system. The central processor of the FPGA system processes and controls the state of the diodes on the unit cells via a 20×20 analog switch drive circuit. After receiving the quantified phase compensation distributions of the unit cells, the FPGA system can independently control the on/off states of the PIN diodes for the antenna spot focusing and scanning at the different locations. Figure 10(b) shows the prototype of the fabricated transmitarray antenna with the control board of the FPGA system.

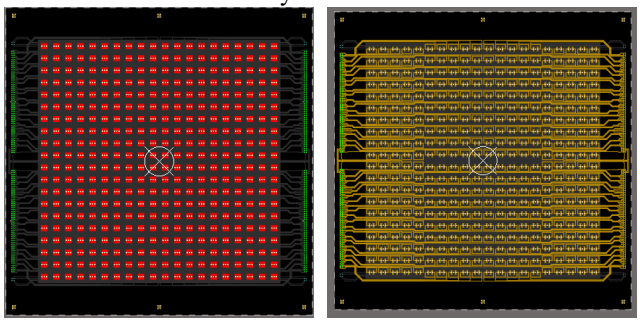

(a) active patch layer (b) Mid layer1

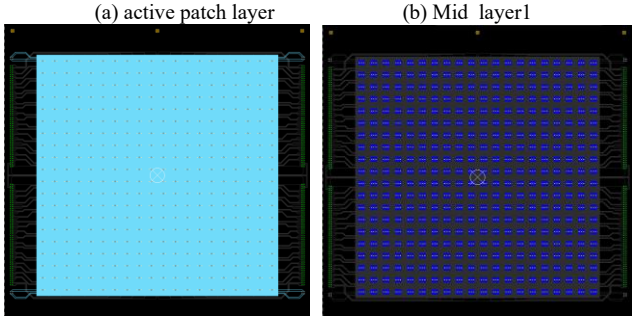

(c) Mid layer2 (d) Bottom layer

Fig. 9. Four layers of the PCB for the implementation.

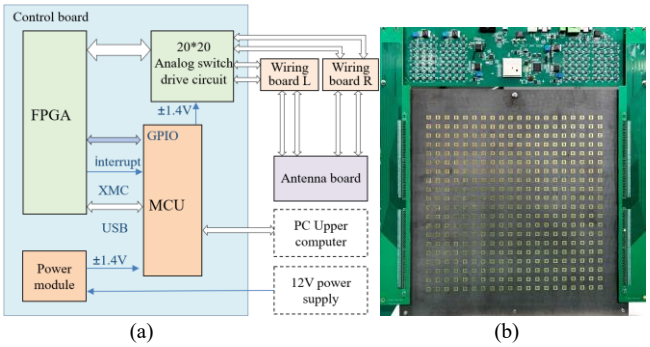

(a) (b)

Fig. 10. (a)Technical specifications for the FPGA control board of the transmitarray antenna; (b) photography of the fabricated transmitarray antenna and the corresponding FPGA control board.

III. Experimental Results

In this section, experimental results are reported to demonstrate the performance of the food contaminant

detection using the proposed MWS system.

Figure 11 shows the experimental scenario diagram for the detection of the low-density contaminants in the static oil-filled food jars using the proposed MWS system. The distance between the two transmitarray antennas is 1 m and the cylindrical food jar in diameter of 8 cm and height of 18 cm is placed along the central axis between two antennas. The scanning position of the focus spot of the transmitarray antennas shifts from 40 cm to -40 cm along the horizonal direction at 9 positions. The interval between two neighboring locations is 10 cm. Assuming that the normal speed of a production line is around 0.5m/s [10] and the interval between two neighboring positions is 0.1m, the time available for measuring one position should be less than 0.2s. We have evaluated that the time for measuring one position and switching to another one is around 20ms, so less than 0.2s. The frequency band 9.5-10.5 GHz is sampled at 11 discrete frequency points with the interval of 100 MHz. We use an upper computer to regulate the different control states of the FPGA systems for the two transmitarray antennas and manually change the position of the food jar at different locations along the central axis to add the samples of the experiment for measuring the S-parameters. The oil jar in the experiment is plastic. It is worth noting that different thicknesses as well as different types of the plastics may influence the electric field distribution inside the food, as thicker plastics with higher permittivity may worsen the near-field focusing performance for the contaminants. However, the issue may only cause a slight impact on the final classification results. This is because the system mainly focuses on the differences of the S parameters data generated by the contaminants, and we don't change the jar. As long as the EM wave can pass through the container and the food, the differences can be captured and correct classifications can be made. Three kinds of the low-density contaminants are considered: a fragment of wood at the upper location, a small splinter of glass at the center location, and a small piece of stone at the bottom location. Figure 12 shows the considered three kinds of the low-density contaminants with their respective locations in the oil-filled food jar. The detailed parameters of the considered contaminants are listed in Table I.

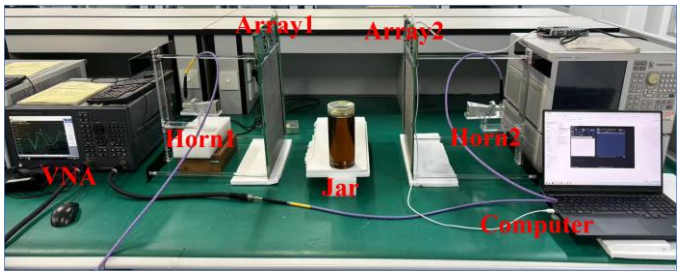

Fig. 11. The distance between the two arrays is 1m, and the jar is moved to different positions in the middle of the two arrays within the system's detection range (40cm to -40cm from the center of the detection domain). The interval between each movement is approximately 10cm.

Fig. 12. The oil jar with contaminants considered in the experiment. The fragment of wood is placed on the upper part of the jar, the small splinter of glass is placed in the center and the stone is placed at the lower part.

TABLE I
TYPICAL VALUES OF RELATIVE PERMITTIVITY AND CONDUCTIVITIES FOR OIL AND OTHER CONTAMINATION MATERIALS

Material	Relative permittivity	Conductivity (S/m)
Oil	2.7-3	0.5
Glass	4.7-10	0.01
Wood	2-16	0.03
Stone	6-10	0.09

The dielectric properties of materials under study at 10 GHz are missing the dielectric losses. We have measured the penetration depth for oil which is ranging from 3.2 cm to 4.5 cm within the frequency 10.5 GHz to 9.5 GHz and around 3.7 cm under 10 GHz. As the radius of the jar in the experiment is 4 cm, after the electromagnetic wave passing through the jar the energy will be severely reduced. Therefore, the transmitarray is applied to increase the near-field electric field intensity inside the jar.

A. Transmitarray Antenna Near-Field

As the first experiment, we investigate the near-field performance of the transmitarray antenna at 10 GHz. The near-field experimental scenario of this experiment is presented in Fig. 13. The electric field is measured within the rectangular experiment plane in size of 10×20 cm located 50 cm away from the transmitarray antenna. We take three positions with 10 cm, 0 cm, and -10 cm shifting from the center of the transmitarray antenna along the horizonal direction. For each experiment plane, we measure the electric field for the spots focused at the upper, center, and lower locations with the interval of 6 cm along the vertical direction.

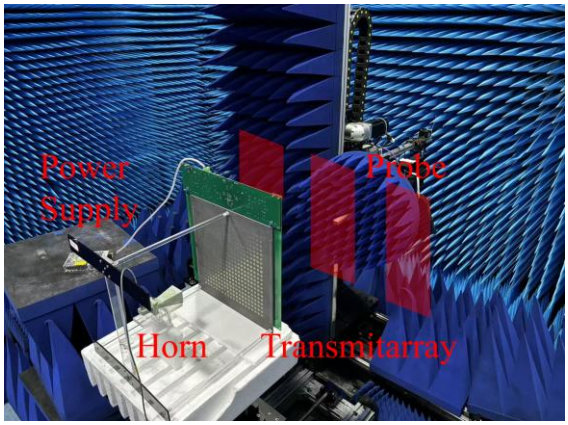

Fig. 13. The near-field experimental scenario in the anechoic chamber. The rectangular areas highlighted in red are the three testing planes at the left, center and the right positions.

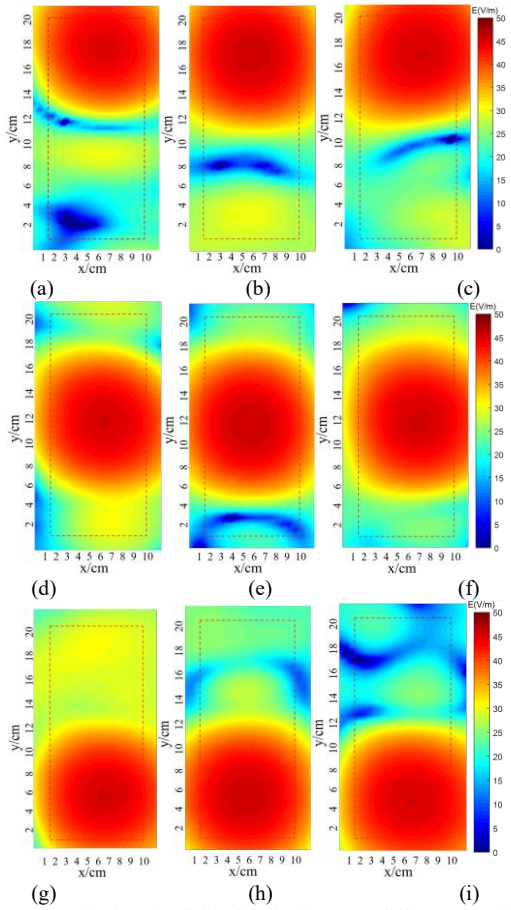

Fig. 14. Measured electric field distributions at different positions. The adjacent position on the left side of the middle position ((a), (d), (g)); the middle position ((b), (e), (h)) and the adjacent position on the right side of the middle position((c), (f), (i)). The red dashed box marks the cross section of the jar.

Figure 14(a)-(i) presents the measured electric field within the experiment planes for the spots focused at the three locations, where the cross section of the cylindrical food jar is denoted using the red dashed line. The figures clearly show that the spot is focused at the expected locations and the width of the spot can almost cover that of the cross section of the cylindrical food jar. From the comparison between the simulations in Fig. 6 and the measurements in Fig. 14, we find that when using the same quantified phases, the measured electric fields at different focusing positions are similar and consistent with the simulated fields, indicating that the focusing strategy is effective in the following experiment. In addition, Fig. 15 shows the measured electric field within the experiment plane for the spot focused at the center position using only the horn antenna (without the transmitarray antenna). Similar as the comparison of the numerical simulation results in Sect. III, the electric field is higher with the use of the transmitarray antenna than that using only the horn antenna. Taking the middle position as an example, the maximum amplitude of the electric field in Fig. 14(d)-(f) is 20.7%, 21.1%, and 20.9% greater than that in Fig. 15. Therefore, the electric field at the detection locations using the designed transmitarray antenna with the larger detection coverage is higher than that using only the horn antenna.

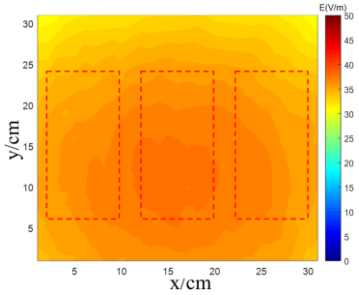

Fig. 15. Electric field distributions of the horn. The electric field is tested within a square plane of 30cm×30cm. The red dashed boxes mark the cross section of the jar at the left, center and the right position as presented in Fig. 13.

B. Generation of Datasets for the ML-Based Contaminant Detection using the MWS System

Next, we present the generation of datasets for the ML model for the detection of the low-density contaminants in the static oil-filled food jars using the proposed MWS system. For each position of the food jar at each frequency point, the measured transmission S-parameter (S_{12} or S_{21}) datasets consist of totally 2000 samples, where 500 samples are obtained for the food jars without the contaminations and 500 samples are obtained for the food jars with each kind of the contaminants as shown in Fig. 12. The measuring time of a single sample for each position is less than 500 ms, allowing measurements in the fast production line in the future dynamic experiment.

Figure 16 (a)-(i) compare the average value (in dB) of the magnitude of the measured S_{12} parameter datasets of the food jar with and without the contaminant (a small piece of stone at the bottom location) for the antenna spot focused at the center location of the food jar placed at the 9 positions along the production line with respect to the frequency. Here, the error bar at each data point represents the range between the measured maximum and minimum S_{12} parameters. These figures show that there are differences between the S-parameters of the food jar with and without the contaminant, which demonstrates the correctness of the analysis of the application of the MWS system in Sect. II-A.

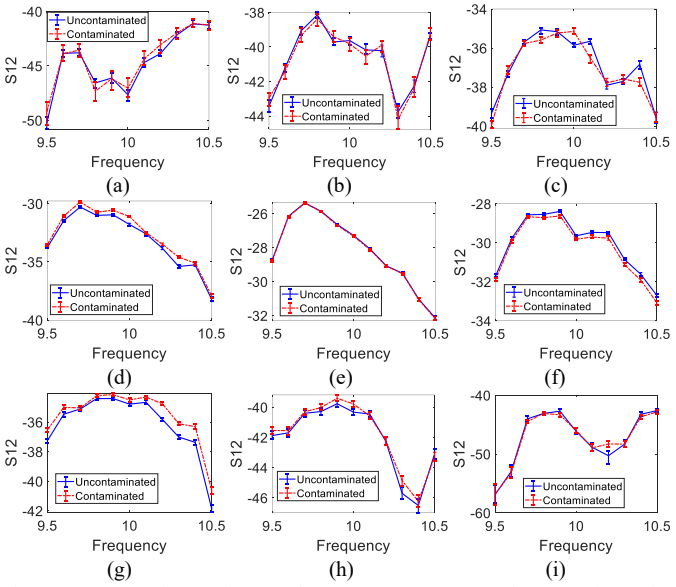

Fig. 16. Measured magnitudes of S-parameters measured across the entire dataset of contaminated samples with a small splinter of stone denoted by the red curves and uncontaminated samples denoted by the blue curves when the jar is at 9 positions along the production line mentioned in the previous experiment set up description from (a) to (i). The error bars are used to represent the effect of noise and operational errors.

To quantify the comparison between the S-parameters obtained for the food jar with and without the contaminant, we further introduce the matrices obtained using the measured S-parameters of the food jar with and without the contaminant. For the processing of the complex S-parameter values for the ML model, we consider both the real and imaginary parts of the S-parameters resulting in a real matrix in size of 18×11. Figure 17(a)-(c) presents the real matrix with the largest l_2-norm among the matrices obtained using the differences between the samples and average values of the measured S-parameters of the food jar without the contaminant, the real matrix with the largest l_2-norm among the matrices obtained using the differences between the samples and average values of the measured S-parameters of the food jar with the contaminant, and the real matrix obtained using the differences between the average values of the measured S-parameters of the food jar with and without the contaminant, respectively. The l_2-norm values of the matrices in Fig. 17(a)-(c) are $1.37e^{-4}$, $1.18e^{-4}$, and $3.92e^{-4}$, respectively. Since the l_2-norm value of the matrix in Fig. 17(c) is larger than the other two values for Fig. 17(a) and (b), we can claim that the existence of the contaminant in the food jar introduces a larger disturbance of the S-parameters for the food jar without the contaminant than the measurement error (noise) of the samples of the S-parameters for the food jar with and without the contaminant, which demonstrates the feasibility of the use of the difference of the S-parameters of the food jars for the identification of the existence of the contaminant as mentioned in Section II-A.

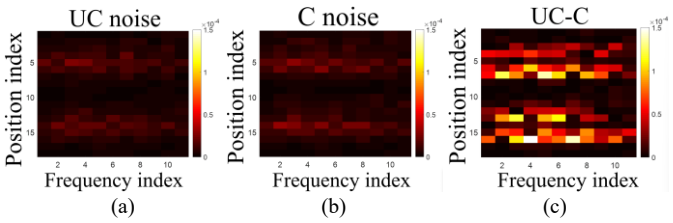

Fig. 17. Comparison of the maximum error matrix of (a) the uncontaminated case, (b) the contaminated case and (c) the difference between the uncontaminated mean value matrix and the contaminated mean value matrix. The abbreviation *UC* and *C* denote the uncontaminated and the contaminated respectively.

C. Training and Testing of the Neural Network for the ML-Based Contaminant Detection using the MWS System

Then, we present the construction of the NN for the ML-based contaminant detection using the proposed MWS system. The designed NN is composed of one multilayer perceptron (MLP) [14]. The ML model is developed in Jupyter Notebook with Python 3.8.16 based on the PyTorch 1.13.1 framework for the model definition, training and predictions.

In the following, we present the training and testing of the neural network (NN) for the ML-based contaminant detection using the MWS system. We design a four-case classifier for the NN to distinguish the food jars without the contaminant and those with the three kinds of the contaminants. Four cases for the food jar are considered: (1) the food jar without the contaminant, (2) the food jar with a fragment of wood at the upper location, (3) the food jar with a small splinter of glass at the center location and (4) the food jar with a small piece of stone at the bottom location. The whole datasets generated in Sect. IV-B are divided into three subsets: training set (53%), validation set (22%), and testing set (25%). The designed NN is trained using the Adam optimizer with a batch size of 8. The initial learning rate is 0.0005. All the training and testing of the NN are carried out on the computer with Intel Xeon Silver 4114 CPU.

In the following, we plot the accuracy of the prediction of the NN using the training and validation sets (using the matrices in size of 18×11 mentioned in Section IV-B) during the training and validation processes. Fig. 18(a) to (c) show the accuracy curve during the training without the focusing strategy (using the horn antenna without the array), with the focusing strategy along horizontal direction only and with the focusing strategy along both the horizontal and vertical directions, respectively. The figures clearly show that 100% accuracy of the prediction of the NN can be eventually achieved for both horizontal and vertical focusing strategy while about 99% for the horizontal focusing only strategy. As a comparison to the focusing strategy, the model exhibits much worse performance without the transmitarray as shown in Fig. 18(a) where the training set and the validation set do not converge to a sufficiently high level of accuracy.

Finally, we investigate the prediction performance of the NN based on the testing set. We introduce the confusion and recall matrices in size of 4×4 for the considered four-classification problem. In Fig. 18, C0 refers to the uncontaminated cases; C1 refers to the glass contaminated cases; C2 refers to the wood contaminated cases and C3 refers

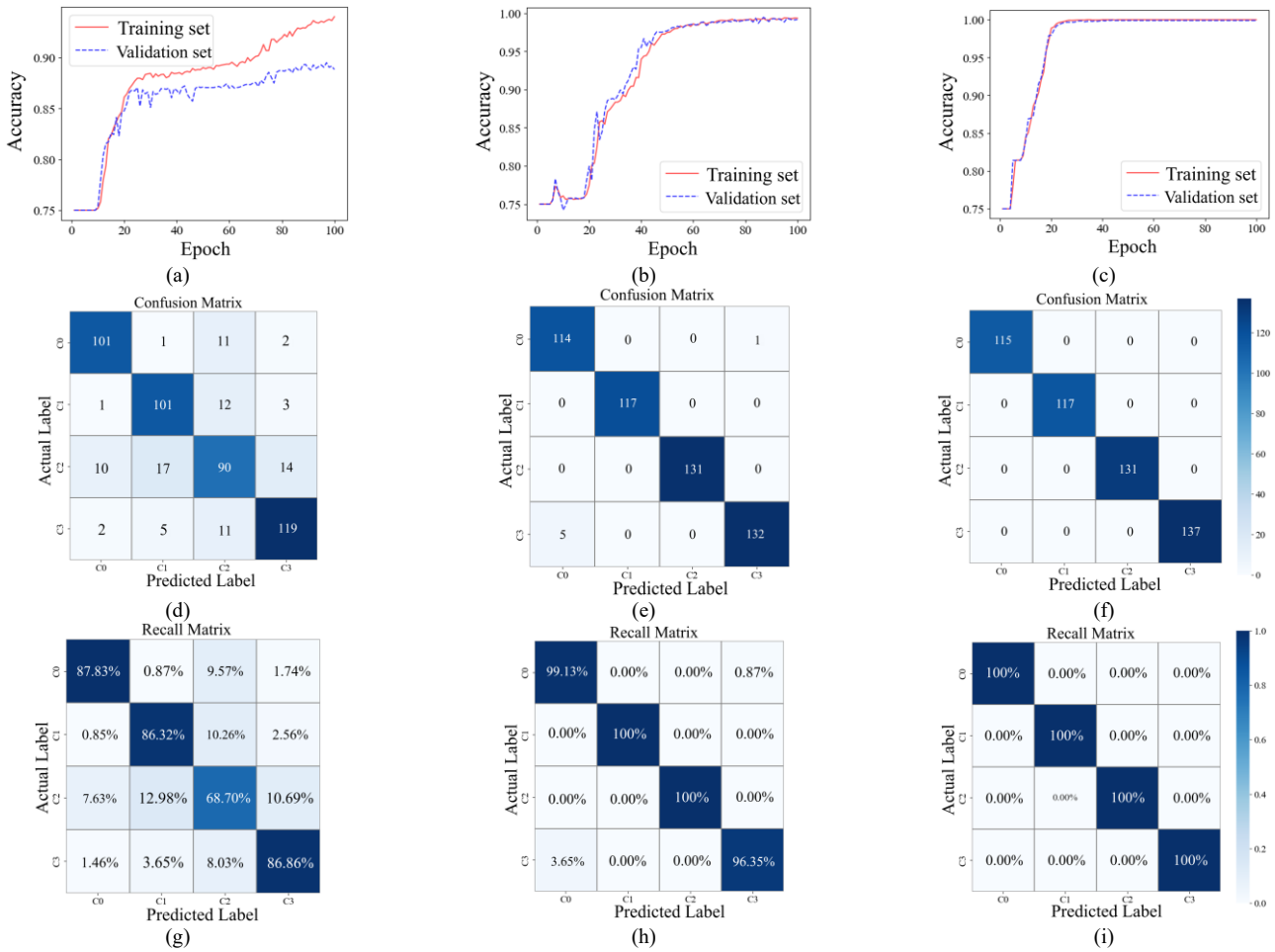

Fig. 18. Accuracy curves during the training (a) without focusing; (b) along the horizontal direction only and (c) along both the horizontal and vertical directions. Confusion matrix in the form of (d)-(f) specific numbers for different cases and (g)-(i) relative percentages (recall matrix) for the two focusing strategies and the strategy without focusing. The samples are all obtained from the splitting of the original experimental dataset.

to the stone contaminated cases. The values of the elements at the m-th row and n-th column in a confusion or a recall matrix denote the number or the relative percentage of the prediction using the NN by predicting the m-th case of the food jar as the n-th case of the food jar as shown in Fig. 18(d) to (i) according to different cases described in Fig 18(a) to (c). It can be clearly seen from the figures that the accuracy of the prediction of the four cases of the food jar is exact 100% for the focusing strategy along both the horizontal and vertical directions, while there are some minor misjudgments for the uncontaminated and contaminated with the small piece of stone for the focusing strategy along only the horizontal direction. Meanwhile, the accuracies are below 90% for all kinds of contaminations using only the horn antennas without the array as shown in Fig. 18(d) and (g).

Cases with respect to more types of contaminants with different sizes and more than one contaminant are studied to further validate the MWS system. Here we conduct an additional experiment with focusing along horizontal directions and the contaminants are with different sizes and quantities, where two stones are involved as shown in Fig. 19. Then the classification results are given in Fig. 20. Here, C0 refers to the uncontaminated cases; C1 refers to the glass contaminated cases; C2 refers to the wood contaminated cases and C3 refers to the two stones contaminated cases.

Fig. 19. The contaminants considered in the additional experiment. (a) The wood is placed on the upper part of the jar, (b) the glass and (c) the two stones are placed at the bottom.

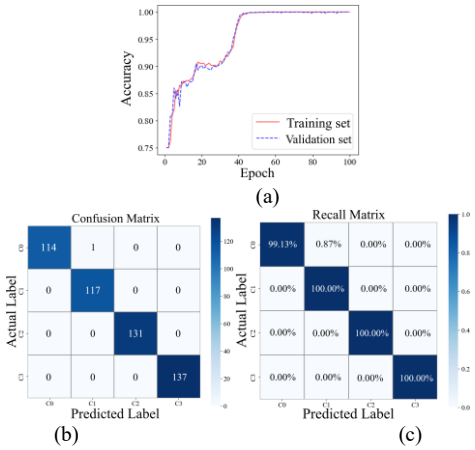

Fig. 20. (a) Accuracy curves during the training. (b) The confusion matrix. (c) The recall matrix.

TABLE II
COMPARISONS OF THE PROPOSED SYSTEM WITH OTHER SIMILAR SYSTEMS

Application	Reference	Purpose	Antenna	Results
-	[24]	Array design	Transmit-array	17.9% 3dB gain bandwidth with maximum 31.14 dBi gain
Medical imaging	[25]	Breast imaging	Transmit-array	Array with a breast imager
Food inspection	[8]	Contaminant imaging	Horn antennas	The initial design, validation, and testing of a system for packaged food
	[10]	Contaminant imaging	Printed antennas	A new design of a multiantenna system with an illumination balancing algorithm
	[27]	Contaminant imaging	Vivaldi antennas	Imaging system for different food materials
	Proposed	Contaminant identification	Transmit-array	A new design of a transmit-array system with machine learning for identification

From Fig. 20 it can be seen that the MWS system is also capable for other types of contaminants.

IV. CONCLUSION AND PERSPECTIVES

In this paper, we proposed a novel MWS system for the detection of the low-density contaminants in food jars. The proposed MWS system was composed of a pair of radiating and receiving horn antennas, two transmitarray antennas integrated with the FPGA control systems, and a VNA for measuring the S-parameters of the food jars. By manipulating the phase of the unit cells of the transmitarray antenna by

switching the on/off states of the PIN diodes on the unit cells, the spots of the antennas can be scanned and focused at the different locations and parts of the food jars along the horizontal and vertical directions. We presented simulation results first to demonstrate that the electric field inside the food jar using the transmitarray antennas is higher than that using only the horn antennas. Then, we conducted the near-field experiment results for the transmitarray antenna to investigate its near-field performance. Finally, we developed a ML-based NN for the detection and classification of the four cases of the static oil-filled food jars and conducted another experiment for generating ML data. The construction of the

NN and the training and testing results of the NN were presented in details. Experiment results without and with different focusing strategies demonstrated the higher accuracy of the proposed MWS system over the existing standard non-focusing system. As mentioned in the introduction, some similar microwave systems have been proposed for other applications. We conclude the relevant literatures in Table II to better illustrate the novelty of the proposed system.

The future works include the development of 2-bit transmitarray antennas for a more precise manipulation of the spot focusing and scanning, and the extension of this work to the application of the MWS system for the contaminant detection for the inline food jars in dynamic real-time is in process.

REFERENCES

[1] M. Edwards, *Detecting Foreign Bodies in Food*. Sawston, U.K.: Wood head Publishing, 2004.

[2] W.-H. Lee and W. Lee, "Food inspection system using terahertz imaging," *Microw. Opt. Technol. Lett.*, vol. 56, no. 5, pp. 1211–1214, 2014.

[3] O. Schimmer, F. Daschner, and R. Knochel, "UWB-sensors in food quality management: The way from the concept to market," *Proc. IEEE Int. Conf. Ultra-Wideband*, pp. 141–144, 2008.

[4] R. Haff and N. Toyofuku, "X-ray detection of defects and contam inants in the food industry," *Sens. Instrum. Food Qual. Saf.*, vol. 2, pp. 262–273, Jun. 2008.

[5] Z. Wu and H. Wang, "Microwave tomography for industrial process imaging: Example applications and experimental results," *IEEE Anten nas Propag. Mag.*, vol.59, no.5, pp.61–71, Oct.2017.

[6] K. Wang, D.-W. Sun, and H. Pu, "Emerging non-destructive terahertz spectroscopy imaging technique: Principle and applications in the agri-food industry," *Trends Food Sci. Technol.*, vol. 67, pp. 93–105, Sept. 2017.

[7] J. LoVetri, M. Asefi, C. Gilmore, and I. Jeffrey, "Innovations in electromagnetic imaging technology: The stored-grain-monitoring case," *IEEE Antennas Propag. Mag.*, vol.62, no.5, pp.33–42, Oct.2020.

[8] J. A. Tobon Vasquez, R. Scapaticci, G. Turvani, M. Ricci, L. Farina, A. Litman, M. R. Casu, L. Crocco and F. Vipiana, "Noninvasive inline food inspection via microwave imaging technology: An application example in the food industry," *IEEE Antennas Propag. Mag*., vol. 62, no. 5, pp.18–32, Oct. 2020.

[9] F. Zidane, J. Lanteri, J. Marot, L. Brochier, N. Joachimowicz, H. Roussel and C. Migliaccio, "Nondestructive control of fruit quality via millimeter waves and classification techniques: Investigations in the automated health monitoring of fruits," *IEEE Antennas Propag. Mag.*, vol.62, no.5, pp. 43–54, Oct. 2020.

[10] M. Ricci, J. A. T. Vasquez, R. Scapaticci, L. Crocco and F. Vipiana, "Multi-antenna system for in-line food imaging at microwave frequencies," *IEEE Trans. Antennas Propag.*, vol. 70, no. 8, pp. 7094-7105, Aug. 2022.

[11] F. Vipiana, L. Crocco, J. LoVetri, "Electromagnetic imaging and sensing for food quality and safety assessment," *IEEE Antennas Propag. Mag.*, vol. 62, no. 5, pp. 16-17, Oct. 2020.

[12] Jeong N, Gan Y and Kong, L, "Emerging non-invasive microwave and millimeter-wave imaging technologies for food inspection", *Critical Reviews in Food Science and Nutrition,* vol. 65, no. 17, pp. 3302-3313, Jul. 2024.

[13] A. Darwish, M. Ricci, J. Tobon, C. Migliaccio, and F. Vipiana, "Near-field microwave sensing technology enhanced with machine learning for the non-destructive evaluation of packaged food and beverage products", *Scientific Reports,* 14:13413, 2024.

[14] M. Ricci, B. Štitić, L. Urbinati, G. D. Guglielmo, J. A. T. Vasquez, L. P. Carloni, F. Vipiana and M. R. Casu, "Machine-learning-based microwave sensing: A case study for the food industry," *IEEE J. Emerg. Sel. Top. Circuits Syst.*, vol. 11, no. 3, pp. 503-514, Sept. 2021

[15] L. Zhou, C. Zhang, F. Liu, Z. Qiu, and Y. He, "Application of deep learning in food: A review," *Comprehensive Rev. Food Sci. Food Saf.*, vol. 18, no. 6, pp. 1793–1811, Nov. 2019.

[16] F. Zidane, J. Lanteri, L. Brochier, N. Joachimowicz, H. Roussel, and C. Migliaccio, "Damaged apple sorting with mmWave imaging and nonlinear support vector machine," *IEEE Trans. Antennas Propag.*, vol. 68, no. 12, pp. 8062–8071, Dec. 2020.

[17] J. Zhang, D. Du, Y. Bao, J. Wang, and Z. Wei, "Development of multifrequency-swept microwave sensing system for moisture measurement of sweet corn with deep neural network," *IEEE Trans. Instrum. Meas.*, vol. 69, no. 9, pp. 6446–6454, Sep. 2020.

[18] Daniel Guyer, Xiukun Yang, "Use of genetic artificial neural networks and spectral imaging for defect detection on cherries", *Comput Electron Agr*, vol. 29, no. 3, pp. 179-194, 2000.
[19] K. T. Pham, A. Clemente, D. Blanco and R. Sauleau, "Dual-Circularly Polarized High-Gain Transmitarray Antennas at Ka-Band," *IEEE Trans. Antennas Propag.,* vol. 68, no. 10, pp. 7223-7227, Oct. 2020.
[20] S. V. Hum and J. Perruisseau-Carrier, "Reconfigurable Reflectarrays and Array Lenses for Dynamic Antenna Beam Control: A Review," *IEEE Trans. Antennas Propag.*, vol. 62, no. 1, pp. 183-198, Jan. 2014.
[21] C. Huang, W. Pan, X. Ma, B. Zhao, J. Cui and X. Luo, "Using Reconfigurable Transmitarray to Achieve Beam Steering and Polarization Manipulation Applications," *IEEE Trans. Antennas Propag.*, vol. 63, no. 11, pp. 4801-4810, Nov. 2015.
[22] F. Diaby, A. Clemente, R. Sauleau, K. T. Pham and L. Dussopt, "2 Bit Reconfigurable Unit-Cell and Electronically Steerable Transmitarray at Ka -Band," *IEEE Trans. Antennas Propag.*, vol. 68, no. 6, pp. 5003-5008, June 2020.
[23] Z. H. Cao, X. Y. Zhang, F. Vipiana, M. R. Casu, G. Turvani, P. F. Gu, R. Chen, M. M. Li, D. Z. Ding,"Design and Beam Optimization of a Novel 1-bit Transmitarray Antenna," *2024 IEEE International Symposium on Antennas and Propagation (AP-S)*, Florence, Italy, July 2024.
[24] M. Alzidani, I. Afifi and A. -R. Sebak, "Design of Wideband Linearly Polarized 3-Bit Transmit-Array Antenna With Polarization Rotation Unit Cell," *IEEE Access*, vol. 9, pp. 113393-113402, 2021.
[25] N. V. Shahmirzadi, A. D. Pitcher, N. K. Nikolova and C. -H. Chen, "Transmitting Array for an Electronically Switched Microwave Breast Imager," *IEEE Trans. Antennas Propag.*, vol. 73, no. 10, pp. 7436-7449, Oct. 2025.
[26] Abbosh, Amin and Afsari, Arman (2024). Stroke monitoring. US20220079443A1.
[27] Bellizzi, Gennaro, Alessio Buzzin, Lorenzo Crocco, Antonio Mastrandrea, Noemi Zeni, Sabrina Zumbo, and Marta Cavagnaro, "A Simple Microwave Imaging System for Food Product Inspection through a Symmetry-Based Microwave Imaging Approach" *Sensors.,* vol. 24, no. 1: 99, Dec 2023.

Yuhan Zuo received the B.S. degree in electronic information engineering from the Nanjing University of Science and Technology, Nanjing, China, in 2021. He is currently pursuing the double Ph.D. degree in electronic science and technology with the Nanjing University of Science and Technology and the Politecnico di Torino, Turin, Italy. His research interests include electromagnetic scattering analysis, computational electromagnetics, and fast integral equation solvers.

Qijian Lu received the B.E. degree in electronic information engineering from the Taizhou Institute of Science and Technology, Nanjing University of Science and Technology, Taizhou, China, in 2022, and the M.S. degree in new generation electronic information technology from Nanjing University of Science and Technology, Nanjing, China, in 2025. His research interests include transmitarray antennas, reflectarray antennas, and metasurface antennas.

Weiliang Yu received the B.E. degree in electronic information engineering from Henan University of Technology, Zhengzhou, China, in 2023. He is currently pursuing the M.S. degree in electronic science and technology at Nanjing University of Science and Technology, Nanjing, China. His current research interests include microwave and millimeter-wave antenna design.

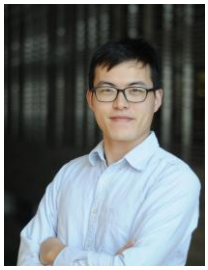

Rui Chen (Member, IEEE) received the B.S. degree in Communication Engineering and the M.S. degree in Electromagnetic Field and Microwave Technology from Nanjing University of Science and Technology (NJUST), China, in 2010 and 2015, respectively, and the Ph.D. degree in Electrical and Computer Engineering from King Abdullah University of Science and Technology (KAUST), Saudi Arabia, in 2021, under the supervisory of Prof. Hakan Bagci.

From 2021 to 2022, he was a Postdoctoral Fellow with the Computational Electromagnetics Group at KAUST. From 2022 to 2023, he was a Postdoctoral Fellow with the Computational Electromagnetics Research Laboratory at Politecnico di Torino, Italy under the mentory of Prof. Francesco P. Andriulli. Since June 2023, he has been an Associate Professor with the School of Microelectronics at NJUST.

His research interests include various aspects of theoretical and applied computational electromagnetics and acoustics with emphasis on frequency- and time-domain surface and volume integral equation methods, fast algorithms, low-frequency analysis, EDA for integrated circuits, quantum computing, brain-computer interface, and geophysical characterization.

Dr. Chen received the Young Scientist Award at International Union of Radio Science (URSI) General Assembly and Scientific Symposium in 2021 and the Honorable Mention Student Paper Competition Awards at IEEE International Symposium on Antennas and Propagation in 2018 and 2020, and the Finalist Student Paper Competition Award at Applied Computational Electromagnetics Society (ACES) Annual Conference in 2019. He was the co-recipient of the Best Student Paper Competition Award (3rd Place) at IEEE International Symposium on Antennas and Propagation in 2023 and the Gauss Centre for Supercomputing Award (Best Paper Award) at International Conference on High Performance Computing in 2020.

He is a Member of Board of Directors of Applied Computational Electromagnetics Society (ACES), a Senior Member of International Union of Radio Science (URSI) and The Electromagnetics Academy, a Member of IEEE Antennas and Propagation Society (AP-S), IEEE Engineering Medicine and Biology Society (EMBS), ACES, The Institution of Engineering and Technology (IET), and a Guest Member of

The European Association on Antennas and Propagation (EurAAP).

Dr. Chen serves as an Associate Editor of *ACES Journal*, a Lead Guest Editor of *Electronics Letters*, and the Technical Program Committee Member and Conference/Session Organizer for many professional society international conferences.

Peng-Fei Gu (Member, IEEE) was born in Nanjing, China. He received the B. S. degree in Electronic Engineering and Ph. D. degree in electromagnetic field and microwave technique from the School of Electrical Engineering and Optical Technique, Nanjing University of Science and Technology, Nanjing, China, in 2012 and 2019, respectively.

From 2019 to 2021, he worked as a postdoctoral researcher of communication engineering at the Nanjing University of Science and Technology. Since 2021, he has been with the School of Microelectronics, Nanjing University of Science and Technology, where he has been an Associate Professor, and a Professor, since 2025. He has authored or coauthored over 100 papers in peer-reviewed international journals and conference proceedings. His current research interests include computational electromagnetics, electromagnetic scattering and radiation, array optimizations, array sparse, metamaterial and stealth design. Prof. Gu is serving as a reviewer for several international journals, including the IEEE Transactions on Antennas and Propagation, IEEE Antennas and Wireless Propagation Letters, IEEE Open Journal of Antennas and Propagation.

Mengmeng Li (M'15–SM'19) received the B.S. degree (Hons.) in physics from Huaiyin Normal College, Huai'an, China, in 2007, and the Ph.D. degree in electromagnetic field and microwave technology from the Nanjing University of Science and Technology, Nanjing, China, in 2014. From 2012 to 2014, he was a Visiting Student with the Electronics Department, Politecnico di Torino, Turin, Italy, and also with the Antenna and EMC Laboratory (LACE), Istituto Superiore Mario Boella, Turin, where he carried out fast solver for multiscale simulations. Since 2014, he has been with the Department of Communication Engineering, Nanjing University of Science and Technology, where he has been an Assistant Professor, Associate Professor, and Professor since 2020. In 2017, he was a Visiting Scholar with Pennsylvania State University, Pennsylvania, PA, USA. His current research interests include computational electromagnetics for electromagnetic fields and scattering, space-time-modulated array design, and automatic target recognition.

Dr. Li was a recipient of the National Science Fund for Excellent Young Scholars in 2022, the Young Scientist Award at the ACES-China Conference in 2019, the Doctoral Dissertation Award of Jiangsu Province in 2016, and ten student paper/contest awards at the international conferences with the students. He is an active reviewer for many IEEE journals and conferences. He is an Associate Editor of the IEEE Antennas and Propagation Magazine, IEEE Open Journal of Antennas and Propagation (OJAP), and a Guest Editor of OJAP.

Francesca Vipiana (M'07–SM'13) received the Laurea and Ph.D. degrees in electronic engineering from the Politecnico di Torino, Torino, Italy, in 2000 and 2004, respectively, with doctoral research carried out partly at the European Space Research Technology Center, Noordwijk, The Netherlands. From 2005 to 2008, she was a Research Fellow with the Department of Electronics, Politecnico di Torino. From 2009 to 2012, she was the Head of the Antenna and EMC Laboratory, Istituto Superiore Mario Boella, Torino. Since 2012, she has been an Assistant Professor with the Department of Electronics and Telecommunications, Politecnico di Torino, where she has been an Associate Professor since 2014 and a Full Professor since 2021.

Her main research activities concern numerical techniques based on integral equations and method of moments, with a focus on multiresolution and hierarchical schemes, domain decomposition, preconditioning and fast solution methods, advanced quadrature integration schemes, and analysis of glide-periodic structures. Moreover, her research interests include the modeling, design, realization and testing of microwave imaging and sensing systems for medical and industrial applications.

She received the Lot Shafai Mid-Career Distinguished Award from the IEEE Antennas and Propagation Society (AP-S) in 2017, she was an Associate Editor of the IEEE Transactions on Antennas and Propagation (2018-2024) and the founder and responsible of the Women in Engineering Column in the IEEE Antennas and Propagation Magazine (2019-2024). She is a member of the EurAAP Board of Directors and the Vice-Chair of the IEEE AP-S Expanding Collaboration & Engagement (ECE) committee.

Dazhi Ding (SM' 21) received the B.Sc. and Ph.D. degrees in electromagnetic field and microwave technique from the Nanjing University of Science and Technology (NJUST), Nanjing, China, in 2002 and 2007, respectively. In 2005, he was with the Center of wireless Communication, City University of Hong Kong, Hong Kong, as a Research Assistant. He joined the Department of Electrical Engineering, NJUST, where he became a Lecturer in 2007. In 2014, he was

promoted to Full Professor in NJUST, where he was appointed as the Head of the Department of Communication Engineering, in September 2014. He is the author or coauthor of over 30 technical articles. He has authored or coauthored more than 80 articles. His current research interests include computational electromagnetics and electromagnetic scattering and radiation. Dr. Ding was a recipient of the National Excellent Youth Fund by the National Science Foundation of China (NSFC) in 2020.